HAL
open science

Hyperspectral super-resolution of locally low rank images from complementary multisource data

Miguel Angel Veganzones, Miguel Simoes, Giorgio Antonino Licciardi, José M. Bioucas-Dias, Jocelyn Chanussot

▶ **To cite this version:**

Miguel Angel Veganzones, Miguel Simoes, Giorgio Antonino Licciardi, José M. Bioucas-Dias, Jocelyn Chanussot. Hyperspectral super-resolution of locally low rank images from complementary multisource data. ICIP 2014 - 21st IEEE International Conference on Image Processing, Oct 2014, Paris, France. pp.n/c, 10.1109/ICIP.2014.7025141 . hal-01010408

HAL Id: hal-01010408

https://hal.science/hal-01010408v1

Submitted on 19 Jun 2014

HAL is a multi-disciplinary open access archive for the deposit and dissemination of scientific research documents, whether they are published or not. The documents may come from teaching and research institutions in France or abroad, or from public or private research centers.

L'archive ouverte pluridisciplinaire **HAL**, est destinée au dépôt et à la diffusion de documents scientifiques de niveau recherche, publiés ou non, émanant des établissements d'enseignement et de recherche français ou étrangers, des laboratoires publics ou privés.

HYPERSPECTRAL SUPER-RESOLUTION OF LOCALLY LOW RANK IMAGES FROM COMPLEMENTARY MULTISOURCE DATA

M.A. Veganzones[1], M. Simões[1,2], G. Licciardi[1], J. Bioucas[2] and J. Chanussot[1,3]

[1]GIPSA-lab, Grenoble-INP, Saint Martin d'Hères, France
[2]Instituto de Telecomunicações, Instituto Superior Técnico, Lisbon, Portugal
[3]Faculty of Electrical and Computer Engineering, University of Iceland, Reykjavik, Iceland

ABSTRACT

Remote sensing hyperspectral images (HSI) are quite often locally low rank, in the sense that the spectral vectors acquired from a given spatial neighborhood belong to a low dimensional subspace/manifold. This has been recently exploited for the fusion of low spatial resolution HSI with high spatial resolution multispectral images (MSI) in order to obtain super-resolution HSI. Most approaches adopt an unmixing or a matrix factorization perspective. The derived methods have led to state-of-the-art results when the spectral information lies in a low dimensional subspace/manifold. However, if the subspace/manifold dimensionality spanned by the complete data set is large, the performance of these methods decrease mainly because the underlying sparse regression is severely ill-posed. In this paper, we propose a local approach to cope with this difficulty. Fundamentally, we exploit the fact that real world HSI are locally low rank, to partition the image into patches and solve the data fusion problem independently for each patch. This way, in each patch the subspace/manifold dimensionality is low enough to obtain useful super-resolution. We explore two alternatives to define the local regions, using sliding windows and binary partition trees. The effectiveness of the proposed approach is illustrated with synthetic and semi-real data.

1. INTRODUCTION

In recent years, there has been a huge improvement of spectral and spatial resolutions in the design of remote sensing sensors. However, it seems that it is not possible to achieve both of them simultaneously. This is due, on the one hand, to the system trade-off related to data volume and signal-to-noise ratio (SNR) limitations and, on the other hand, to the specific requirements of different applications [13]. Then, there is a need for super-resolution techniques that fuse high spectral resolution images, such as hyperspectral images (HSI), with high spatial images such as multispectral images (MSI) or panchromatic images, in order to obtain high spectral and spatial (super-resolution) images.

Recently, some techniques dedicated to the fusion of HSIs and MSIs have been proposed. A general trend is to associate this problem with either linear spectral unmixing, which assumes that the underlying data can be described by a mixture of a relatively small number of "pure" spectral signatures, corresponding to the materials present in the scene or, with the learning of a spectral dictionary that codifies the information present on the images. Since both HSIs and MSIs capture the same scene, the underlying materials (the so-called *endmembers*) or the dictionaries should be the same. Therefore, the spectral information extracted from one of the images should also be able to explain the other one. Due to the high spectral resolution of the HSIs, the endmembers or the dictionary are extracted from these data, and are then used to reconstruct the MSI. Since MSIs have high spatial resolution, the final reconstructed image will be at super-resolution. Hyperspectral super-resolution could improve the results of further analysis, such as super-resolution mapping [14, 15, 21, 23].

1.1. Related work

Zurita *et al.* [24], introduced one of the first unmixing-based approaches to the fusion of remote sensing multiband images. A related approach is proposed in [9], where a very high-resolution hyperspectral image is estimated from a lower-resolution hyperspectral image and a high-resolution RGB image. The method starts by identifying an unmixing matrix used to represent the hyperspectral spectra and then uses this matrix in conjunction with the RGB input to compute, via sparse regression, representation coefficients for the high-resolution hyperspectral image. This methodology can be viewed as a factorization of the input into a mixing matrix and a set of maximally sparse coefficients. An approach with similar flavour is proposed in [6]. The main difference is that the mixing matrix is replaced by a dictionary learnt using a non-negative matrix factorization with sparsity regularization on the code. In [7], the hyperspectral data is unmixed via the K-SVD algorithm, and the multispsectral data is reconstructed using orthogonal matching pursuit to induce sparsity. Authors in [13] proposed a method where two dictionaries were learned from the two different data, and then used a dictionary-pair learning method to establish the correspondence between them. A similar and older technique introduced in [22] alternately unmixes both sources of data to find the signatures and the abundances of the endmembers.

1.2. Contribution

In real world HSI, it is very likely that in a small spatial neighbourhood the number of different materials is small, i.e., these images are locally low rank. We take advantage of this property to propose a local super-resolution methodology. Firstly, we propose two approaches, one using a square sliding window of fixed size and a second using a binary partition tree representation, to obtain a set of patches from the image, such that the set of pixels with indices

Miguel A. Veganzones was supported by ERC AdG-2013-320594 DECODA and by the Delegation Generale de l'Armement (DGA) under contract PDE2012600079. Prof. Bioucas and M. Simões were supported by the Portuguese Science and Technology Foundation under Projects PEst-OE/EEI/LA0008/2013 and PTDC/EEI-PRO/1470/2012, and grant SFRH/BD/87693/2012.

in each patch span a subspace of lower dimensionality than that of the whole image. Secondly, we exploit the locally low rank property of the pixels of each patch by using an endmembers induction algorithm (EIA) to find the low rank subspace spanned by the spectral signatures of the materials present in each patch. The proposed methodology does not need to estimate the spatial blur, as far as it is constant across bands.

1.3. Outline

The remainder of the paper is organized as follows: in Sec. 2 the super-resolution problem is formulated, in Sec. 3 the proposed local super-resolution methodology is introduced and finally, in Sec. 4 experimental results and some concluding remarks are provided.

2. PROBLEM FORMULATION

Let $\mathbf{X} \in \mathbb{R}^{n_h \times n}$ denote a HSI with n_h spectral bands (rows of $\mathbf{X}$) and $n = n_x \times n_y$ pixels (columns of $\mathbf{X}$). We may interpret $\mathbf{X}$ either as a collection of n_h images (or bands) of size $n_x \times n_y$, each one associated to a given wavelength interval, or as a collection of n spectral vectors of size n_h, each one associated with a given pixel. In this work, we are concerned with the estimation of $\mathbf{X}$, which we term the original HSI, from two degraded observations of $\mathbf{X}$: a) a low spatial resolution HSI, $\mathbf{Y}_h \in \mathbb{R}^{n_h \times (n_x/d) \times (n_y/d)}$, where $d > 1$ denotes a spatial downsampling factor, and b) a MSI, $\mathbf{Y}_m \in \mathbb{R}^{n_m \times n_x \times n_y}$, where $n_m \ll n_h$. We assume that $\mathbf{Y}_h$ is generated as

$$\mathbf{Y}_h = \mathbf{XBM} + \mathbf{N}_h, \tag{1}$$

where $\mathbf{B} \in \mathbb{R}^{n \times n}$ is a matrix modeling band independent sensor blur, $\mathbf{M} \in \mathbb{R}^{n \times (n/d^2)}$ is a masking matrix accounting for spatial downsampling of size d on both spatial dimensions, and $\mathbf{N}_h$ is an additive perturbation. Concerning the MSI, $\mathbf{Y}_m$, we assume the generation model

$$\mathbf{Y}_m = \mathbf{RX} + \mathbf{N}_m, \tag{2}$$

where the matrix $\mathbf{R} \in \mathbb{R}^{n_m \times n_h}$ holds in its columns the n_h spectral responses of the multispectral sensor, and $\mathbf{N}_m$ is an additive perturbation.

Let us suppose that it is possible to learn a dictionary $\mathbf{D} \in \mathbb{R}^{n_h \times n_d}$ from the hyperspectral image $\mathbf{Y}_h$, and that the columns $\mathbf{X}$, denoted by $\mathbf{x}_i$, for $i = 1, \ldots, n$, may be sparsely represented as linear combinations of the columns of $\mathbf{D}$. That is, given $\mathbf{x}_i$ for $i \in \mathcal{S}$, there is a sparse vector $\boldsymbol{\alpha}_i \in \mathbb{R}^{n_d}$ (*i.e.*, only a few components of $\boldsymbol{\alpha}_i$ are non-zero) such that:

$$\mathbf{x}_i = \mathbf{D}\boldsymbol{\alpha}_i. \tag{3}$$

By replacing (3) in (2), we obtain:

$$\mathbf{Y}_m = \mathbf{RDA} + \mathbf{N}_m, \tag{4}$$

where $\mathbf{A} \equiv [\boldsymbol{\alpha}_1, \ldots, \boldsymbol{\alpha}_n]$, is often termed as *code* in dictionary learning and sparse regression applications. If equation (4) can be solved with respect to $\mathbf{A}$, then we may plug its solution into (3) and thereby obtain an estimate of $\mathbf{X}$.

The success of a dictionary-based approach depends fundamentally on the ability to solve (4) with respect to $\mathbf{A}$. The difficulty in solving this system comes from the fact that the system matrix $\mathbf{RD} \in \mathbb{R}^{n_m \times n_d}$ is often fat, *i.e.*, $n_m < n_d$, yielding an undetermined system of equations. A typical multispectral sensor has less than 10 bands, quite often 4 in the wavelength interval $[0.4, 2.5]$ microns where most hyperspectral sensors operate, whilst n_d is often of the order of a few tens. The ill-posedness of (2) when $n_m < n_d$ may be cured by exploiting the sparsity of the codes $\boldsymbol{\alpha}_i$, for $i \in \mathcal{S}$, which opens the door to all sort of sparse regression techniques, many of them recently introduced in compressive sensing [2] applications. Nevertheless, we still face a difficulty: in hyperspectral applications, the columns of $\mathbf{D}$ tend to be highly correlated, implying that the *mutual coherence* of the columns of $\mathbf{RD}$ is close to 1. This makes (2) ill-posed even when codes $\boldsymbol{\alpha}_i$, for $i \in \mathcal{S}$, are sparse [8, 4].

In the next section, we introduce two local dictionary-based techniques conceived to cope with the ill-posedness with origin in the matrix system $\mathbf{RD}$. The main idea, in the vein of the local approaches to image restoration, is to decompose the HSI into patches and build patch-dependent dictionaries such that $n_m \geq n_d$ in each patch. Thereby, the inverse problem of solving (2) in each patch is well-posed.

3. LOCAL DICTIONARY BASED HSI SUPER-RESOLUTION

3.1. Local spatial patches definition

Let $\mathcal{P}_j$ denote the set of patches obtained from an image, $\mathbf{Y}_h$, such that the set of pixels with indices in each patch, $\mathbf{Y}_j \equiv [\mathbf{y}_i,\ i \in \mathcal{P}_j]$, span a subspace of lower dimensionality than that of $\mathbf{Y}_h$. Next, we introduce two approaches to obtain such patches. The first approach uses a sliding window and the second approach relies on a binary partition tree (BPT) representation [12].

3.1.1. Using a sliding window of fixed size

The sliding window methodology has been broadly used in image processing. It consists in defining a square window of fixed size so the pixels lying inside the window form a patch. The window then slides over the whole image in a standard zig-zag way, be it with some overlapping or not, eventually covering the whole image and defining the image patches, $\mathcal{P}_j$.

3.1.2. Using a BPT representation

The BPT is a hierarchical region-based representation of an image in a tree structure [12]. In the BPT representation, the leaf nodes correspond to an initial partition of the image, which can be the individual pixels, or a coarser segmentation map. From this initial partition, an iterative bottom-up region merging algorithm is applied until only one region remains. This last region represents the whole image and corresponds to the root node. All the nodes between the leaves and the root result of the merging of two adjacent children regions.

Two notions are of prime importance when defining a BPT, the *region model*, $\mathcal{M}_{\mathcal{R}}$, which specifies how a region $\mathcal{R}$ is modelled, and the *merging criterion*, $\mathcal{O}(\mathcal{M}_{\mathcal{R}_\alpha}, \mathcal{M}_{\mathcal{R}_\beta})$, which is a distance measure between the region models of any two regions $\mathcal{R}_\alpha$ and $\mathcal{R}_\beta$. Each merging iteration involves the search of the two neighbouring regions which achieve the lowest pair-wise dissimilarity among all the pairs of neighbouring regions in the current segmentation map. Those two regions are consequently merged. To build the BPT representation from the hyperspectral image [17, 18, 19], $\mathbf{Y}_h$, we use

the first-order parametric model $\mathcal{M}_{\mathcal{R}}$:

$$\mathcal{M}_{\mathcal{R}} \stackrel{d}{=} \bar{\mathbf{x}} = \frac{1}{N_{\mathcal{R}}} \sum_{i=1}^{N_{\mathcal{R}}} \mathbf{x}_i,$$

where $N_{\mathcal{R}}$ is the number of pixels on the region; and, in order to merge regions, the spectral angle distance:

$$\mathcal{O}\left(\mathcal{M}_{\mathcal{R}_\alpha}, \mathcal{M}_{\mathcal{R}_\beta}\right) \stackrel{d}{=} d_{\text{SAM}}\left(\bar{\mathbf{x}}_\alpha, \bar{\mathbf{x}}_\beta\right) = \arccos\left(\frac{\bar{\mathbf{x}}_\alpha \bar{\mathbf{x}}_\beta}{\|\bar{\mathbf{x}}_\alpha\| \|\bar{\mathbf{x}}_\beta\|}\right).$$

Once the BPT representation is built, the BPT is pruned to achieve a partition of the image such that the regions of the partition define the image patches, $\mathcal{P}_j$. We use the vote-based pruning approach from [16], where each region of the BPT representation is voted by its children. A region receives a number of votes equal to the leaves of a children node if the distance between the region model and the children model is above some threshold. Once all the regions have collected their number of votes, the BPT is pruned so the partition cardinality is maximized constrained to the regions of the partition having received at least half the total number of votes.

3.2. Local dictionary-based super-resolution

Given a set of patches $\mathcal{P}_j$, $j = 1, \ldots, P$; for each $\mathcal{P}_j$, we identify a mixing matrix $\mathbf{D}_j$ by applying an EIA to extract a set of endmembers from the set of pixels $\mathbf{X}_j$, identified by the corresponding patch. Having identified the dictionaries, $\mathbf{D}_j$, the code $\mathbf{A}$ is estimated by solving the following constrained least squares (CLS) problems:

$$\min_{\mathbf{A}_j \geq 0} \|\mathbf{Y}_{m,j} - \mathbf{R}\mathbf{D}_j\mathbf{A}_j\|_F^2 \quad j = 1, \ldots, P, \tag{5}$$

where $\mathbf{A}_j \in \mathbb{R}^{n_d \times |\mathcal{P}_j|}$ and $\mathbf{Y}_{m,j} \in \mathbb{R}^{n_m \times |\mathcal{P}_j|}$ gathers, respectively, the columns of $\mathbf{A}$ and $\mathbf{Y}_m$ with indices corresponding to the pixels $\mathbf{X}_j$ in $\mathcal{P}_j$. The inequality $\mathbf{A}_j \geq 0$ is to be understood in the component-wise sense, and $\|\cdot\|_F$ denotes the Frobenius norm. The constraint $\mathbf{A}_j \geq 0$ in (5) is used because, in the linear mixing model, the codes $\boldsymbol{A}_j$ represent abundances of materials which are necessarily non-negative [10]. It is possible to add the abundances sum-to-one constraint, $\mathbf{A}_j^T \mathbf{I} = \mathbf{1}_{|\mathcal{P}_j|}$, but this constraint is usually dropped due to possible scale model mismatches [4]. We remark that, since our observations are spectral vectors and thus non-negative (apart from the noise contribution), the non-negativity constraint in (5) is equivalent to a form of constrained ℓ_1 regularization and therefore, to some kind of sparsity enforcement (see [5] for the details).

In order to solve (5), we use the SUnSAL algorithm [3], which is an instance of the C-SALSA methodology introduced in [1] to effectively solve a large number of CLS problems sharing the same matrix system. Fig. 1 shows the pseudocode of the proposed HSI Super Resolution via Local Dictionary Learning using EIAs (HSR-LDL-EIA). The algorithm operates on each patch independently. Each patch indexes the set of pixels in the hyperspectral image, $\mathbf{Y}_{h,j}$, and in the multispectral image, $\mathbf{Y}_{m,j}$. From the hyperspectral set of pixels, the subspace matrix, $\mathbf{D}_j$, is obtained using any EIA. Then, the SUnSAL algorithm is used to estimate the fractional abundances, $\widehat{\mathbf{A}}_j$, from the multispectral set of pixels. The fractional abundances are linearly combined with the estimated subspace to estimate the super-resolution pixels of the patch, $\widehat{\mathbf{X}}_j$. The estimated super-resolution pixels of all the patches are combined to form the estimated super-resolution image, $\mathbf{X}$.

Algorithm *HSR-LDL-EIA*
Input:
1. $\mathbf{Y}_h, \mathbf{Y}_m, \mathbf{R}, \mathcal{P}_j, n_d$
2. **for** $j = 1$ **to** P
3. $\quad\quad \mathbf{Y}_{m,j} := [\mathbf{Y}_{m,i}, i \in \mathcal{P}_j]$
4. $\quad\quad \mathbf{Y}_{h,j} := [\mathbf{Y}_{h,i}, i \in \mathcal{P}_j]$
5. $\quad\quad \mathbf{D}_j := \text{EIA}(\mathbf{Y}_{h,j}, n_d)$
6. $\quad\quad \widehat{\mathbf{A}}_j := \arg\min_{\mathbf{A}_j \geq 0} \|\mathbf{Y}_{m,j} - \mathbf{R}\mathbf{D}_j\mathbf{A}_j\|_F^2$
7. $\quad\quad \widehat{\mathbf{X}}_j := \mathbf{D}_j\widehat{\mathbf{A}}_j$
8. $\widehat{\mathbf{X}} := \left\{\widehat{\mathbf{X}}_j\right\}, \; j = 1, \ldots, P$

Fig. 1. HSI Super Resolution via Local Dictionary Learning using Endmember Induction Algorithms (HSR-LDL-EIA).

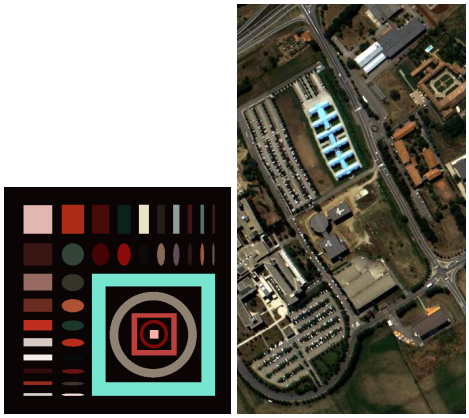

(a) (b)

Fig. 4. False color representations of the experimental datasets: (a) Synthetic dataset and, (b) Pavia University dataset.

4. EXPERIMENTAL RESULTS AND CONCLUSIONS

4.1. Experimental methodology

In order to assess the performance of the proposed local super-resolution methods, we followed the experimental methodology derived from the Wald's protocol proposed in [20]: 1) Given a denoised super-resolution image, $\mathbf{X}$, we simulate a low-spatial resolution hyperspectral image, $\mathbf{Y}_h$, by applying a Gaussian blurring ($\mathbf{B}$) and downsampling the blurred image by a factor of four ($\mathbf{M}$). 2) We also simulate a high-spatial resolution multispectral image, $\mathbf{Y}_m$, by applying a spectral response matrix ($\mathbf{R}$) to the original super-resolution image. 3) White noise was added to both images, $\mathbf{Y}_h$ and $\mathbf{Y}_m$, with $30db$ and $40db$ respectively. 4) Then, we estimate the super-resolution image, $\hat{\mathbf{X}}$, by applying a super-resolution methodology to both images, $\mathbf{Y}_h$ and $\mathbf{Y}_m$. 5) After denoising the estimated super-resolution image, we compare it to the original one using the SAM, the ERGAS and the Q quality measures [13]. The SAM measures the spectral difference being 0 the best. The ERGAS is a spectral-spatial quality measure being 0 the best. The Q index is a correlation measure being 1 the best.

We compared the proposed local super-resolution approach, HSR-LDL-EIA, to the global one, HSR-GDL-EIA, by means of 50 Monte Carlo runs. For the proposed local approach, we also com-

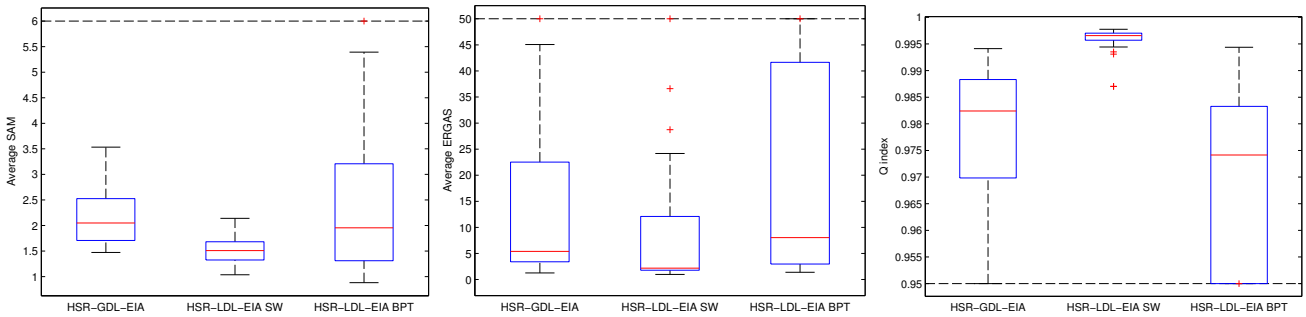

(a) (b) (c)

Fig. 2. Results obtained for the synthetic dataset: (a) Average SAM, (b) Average ERGAS and (c) Q index.

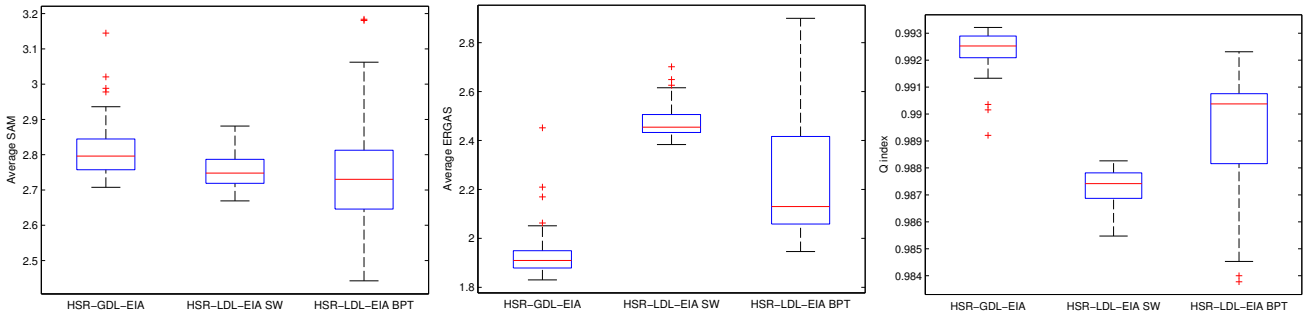

(f) (g) (h)

Fig. 3. Results obtained for the Pavia University dataset: (a) Average SAM, (b) Average ERGAS and (c) Q index.

pared the sliding window (SW) and BPT-based approaches to obtain the image patches. For the SW approach, we set the windows size to 60 with a 0.2% overlap (12 pixels). We used the Vertex Component Analysis (VCA) EIA [11] to induce the set of endmembers.

4.2. Datasets

Synthetic dataset: a synthetic image composed of multiple geometric shapes (ellipses and rectangles) of different sizes and orientations, where each geometrical element and the background are formed using a different linear mixture of 5 endmembers from the USGS spectral library, for a total of 45 different endmembers in the image. This image simulates a high spectral variability scenario. The multi-spectral image was simulated using the spectral response of the Ikonos sensor. In this case, we fixed the number of induced endmembers to $p = 5$ for the local approaches, and $p = 45$ for the global one. Fig. 4a depicts a false color image of the synthetic dataset.

Pavia University dataset: this dataset is a real image representing an urban area mainly composed of buildings, urban vegetation and parking lots. The multi-spectral image was simulated using the spectral response of the first multi-spectral three bands of the Ikonos sensor. For the local approaches, we fixed the number of induced endmembers to $p = 3$. For the global approach, this value was set to $p = 10$. Fig. 4b depicts a false color image of the Pavia University dataset.

4.3. Results and conclusions

Figures 2 and 3 show the results of the 50 Monte Carlo runs obtained for the synthetic and Pavia University datasets respectively. Results show that the local sliding window approache outperforms the global one in the synthetic scene and partially in the Pavia University scene. The local BPT approach shows a potential improving over the global and local sliding window approaches, but it presents a high variance over the Monte Carlo runs. This issue could be due to the effects of noise on the BPT representation or to the voting pruning strategy. The lack of space prevents us from showing the obtained super-resolution images for visual comparison. We encourage the interested reader to access the results extended report at first author's website[1]. We'll further work on the validation of the proposed methodologies and on the study of the patches definition by means of other BPT representations and pruning strategies. We'll also face the problem of estimate the spectral response matrix, $\mathbf{R}$, from the data.

[1] http://www.gipsa-lab.grenoble-inp.fr/page_pro.php?vid=1728

5. REFERENCES

[1] Manya V Afonso, José M Bioucas-Dias, and Mário AT Figueiredo. An augmented lagrangian approach to the constrained optimization formulation of imaging inverse problems. *Image Processing, IEEE Transactions on*, 20(3):681–695, 2011.

[2] Richard G Baraniuk. Compressive sensing [lecture notes]. *Signal Processing Magazine, IEEE*, 24(4):118–121, 2007.

[3] José M Bioucas-Dias and Mário AT Figueiredo. Alternating direction algorithms for constrained sparse regression: Application to hyperspectral unmixing. In *Hyperspectral Image and Signal Processing: Evolution in Remote Sensing (WHISPERS), 2010 2nd Workshop on*, pages 1–4. IEEE, 2010.

[4] José M Bioucas-Dias, Antonio Plaza, Nicolas Dobigeon, Mario Parente, Qian Du, Paul Gader, and Jocelyn Chanussot. Hyperspectral unmixing overview: Geometrical, statistical, and sparse regression-based approaches. *Selected Topics in Applied Earth Observations and Remote Sensing, IEEE Journal of*, 5(2):354–379, 2012.

[5] Alfred M Bruckstein, Michael Elad, and Michael Zibulevsky. On the uniqueness of nonnegative sparse solutions to underdetermined systems of equations. *Information Theory, IEEE Transactions on*, 54(11):4813–4820, 2008.

[6] Adam S Charles, Bruno A Olshausen, and Christopher J Rozell. Learning sparse codes for hyperspectral imagery. *Selected Topics in Signal Processing, IEEE Journal of*, 5(5):963–978, 2011.

[7] Bo Huang, Huihui Song, Hengbin Cui, Jigen Peng, and Zongben Xu. Spatial and Spectral Image Fusion Using Sparse Matrix Factorization. *ieeexplore.ieee.org*, pages 1–12, 2013.

[8] M-D Iordache, José M Bioucas-Dias, and Antonio Plaza. Sparse unmixing of hyperspectral data. *Geoscience and Remote Sensing, IEEE Transactions on*, 49(6):2014–2039, 2011.

[9] Rei Kawakami, Yasuyuki Matsushita, John Wright, Moshe Ben-Ezra, Yu-Wing Tai, and Katsushi Ikeuchi. High-resolution hyperspectral imaging via matrix factorization. *Cvpr 2011*, pages 2329–2336, June 2011.

[10] W.-K. Ma, J.M. Bioucas-Dias, Tsung-Han Chan, N. Gillis, P. Gader, A.J. Plaza, A. Ambikapathi, and Chong-Yung Chi. A signal processing perspective on hyperspectral unmixing: Insights from remote sensing. *Signal Processing Magazine, IEEE*, 31(1):67–81, Jan 2014.

[11] J.M.P. Nascimento and J.M. Bioucas Dias. Vertex component analysis: a fast algorithm to unmix hyperspectral data. *Geoscience and Remote Sensing, IEEE Transactions on*, 43(4):898–910, April 2005.

[12] P. Salembier and L. Garrido. Binary partition tree as an efficient representation for image processing, segmentation, and information retrieval. *Image Processing, IEEE Transactions on*, 9(4):561–576, Apr 2000.

[13] Huihui Song, Bo Huang, Kaihua Zhang, and Hankui Zhang. Spatio-spectral fusion of satellite images based on dictionary-pair learning. *Information Fusion*, 18(0):148 – 160, 2014.

[14] Yuan-Fong Su, G.M. Foody, A.M. Muad, and Ke-Sheng Cheng. Combining hopfield neural network and contouring methods to enhance super-resolution mapping. *Selected Topics in Applied Earth Observations and Remote Sensing, IEEE Journal of*, 5(5):1403–1417, Oct 2012.

[15] Yuan-Fong Su, G.M. Foody, A.M. Muad, and Ke-Sheng Cheng. Combining pixel swapping and contouring methods to enhance super-resolution mapping. *Selected Topics in Applied Earth Observations and Remote Sensing, IEEE Journal of*, 5(5):1428–1437, Oct 2012.

[16] G. Tochon, J. Feret, R.E. Martin, R. Tupayachi, J. Chanussot, and G.P. Asner. Binary partition tree as a hyperspectral segmentation tool for tropical rainforests. In *Geoscience and Remote Sensing Symposium (IGARSS), 2012 IEEE International*, pages 6368–6371, July 2012.

[17] S. Valero, P. Salembier, and J. Chanussot. Comparison of merging orders and pruning strategies for binary partition tree in hyperspectral data. In *Image Processing (ICIP), 2010 17th IEEE International Conference on*, pages 2565–2568, Sept 2010.

[18] S. Valero, P. Salembier, and J. Chanussot. Hyperspectral image representation and processing with binary partition trees. *Image Processing, IEEE Transactions on*, 22(4):1430–1443, April 2013.

[19] M.A. Veganzones, G. Tochon, M. Dalla Mura, A.J. Plaza, and J. Chanussot. Hyperspectral image segmentation using a new spectral mixture-based binary partition tree representation. In *Image Processing (ICIP), 2013 20th IEEE International Conference on*, pages 245–249, Sept 2013.

[20] Lucien Wald, Thierry Ranchin, and Marc Mangolini. Fusion of Satellite Images of Different Spatial Resolutions : Assessing the Quality of Resulting Images. 63(6):691–699, 1997.

[21] Xiong Xu, Yanfei Zhong, Liangpei Zhang, and Hongyan Zhang. Sub-pixel mapping based on a map model with multiple shifted hyperspectral imagery. *Selected Topics in Applied Earth Observations and Remote Sensing, IEEE Journal of*, 6(2):580–593, April 2013.

[22] Naoto Yokoya, Student Member, Takehisa Yairi, and Akira Iwasaki. Coupled Nonnegative Matrix Factorization Unmixing for Hyperspectral and Multispectral Data Fusion. 50(2):528–537, 2012.

[23] Yihang Zhang, Yun Du, Feng Ling, Shiming Fang, and Xiaodong Li. Example-based super-resolution land cover mapping using support vector regression. *Selected Topics in Applied Earth Observations and Remote Sensing, IEEE Journal of*, 7(4):1271–1283, April 2014.

[24] R. Zurita-Milla, J. G P W Clevers, and M.E. Schaepman. Unmixing-based landsat tm and meris fr data fusion. *Geoscience and Remote Sensing Letters, IEEE*, 5(3):453–457, July 2008.